

Relativistic energy loss in a dispersive medium

Jens M. Houlik*

Department of Chemistry and Applied Engineering Science, Aalborg University Esbjerg, Niels Bohrs Vej 8, 6700 Esbjerg, Denmark

(Received 14 March 2002; revised manuscript received 10 May 2002; published 19 August 2002)

The electron energy loss in a dispersive medium is obtained using macroscopic electrodynamics taking advantage of a static frame of reference. Relativistic corrections are described in terms of a dispersive Lorentz factor obtained by replacing the vacuum velocity c by the characteristic phase velocity c/n , where n is the complex index of refraction. The angle-resolved energy-loss spectrum of a Drude conductor is analyzed in detail and it is shown that the low-energy peak due to Ohmic losses is enhanced compared to the classical approximation.

DOI: 10.1103/PhysRevA.66.022901

PACS number(s): 34.50.Bw, 03.30.+p, 41.20.-q

I. INTRODUCTION

The study of charged particles passing through matter has a long history [1,2] and remains of current interest in modern electron energy-loss spectroscopy [3,4]. Energy loss is caused by close-range collisions or many-body excitations in the medium due to polarization and magnetization [5,6]. Slow electrons incident on a metal foil at a velocity much smaller than the Fermi velocity will be screened on a length scale comparable to atomic distances, while screening is expected to be less effective for relativistic electrons. The Lorentz factor of the source electrons,

$$\gamma = (1 - \beta^2)^{-1/2}, \quad (1)$$

where $\beta = v_s/c$ is proportional to the total energy, $\gamma = E_{kin}/mc^2 + 1$, where $mc^2 = 511$ keV is the electron rest energy. A transmission electron microscope (TEM) operated at the energy $E_{kin} \sim 100$ keV, therefore has the typical value, $\gamma \sim 1.2$, corresponding to $\beta \sim 0.5$. Relativistic effects can therefore be expected in the energy-loss spectrum [7–9].

Semiclassically, an excited mode corresponds to the energy loss $\hbar\omega \ll E_{kin}$ and momentum transfer $\hbar k \ll \gamma m v_s$, where the deflection angle

$$\alpha = \hbar k_{\perp} / \gamma m v_s \quad (2)$$

is the ratio of the electron de Broglie wavelength to the length scale, $\lambda_{\perp} = 2\pi/k_{\perp}$, measuring the size of excitations perpendicular to the electron path. Since the Compton wavelength has the value $h/mc = 0.024$ Å, the macroscopic excitations will in general have small scattering angles.

The detailed geometry of the sample introduces further structure in the loss spectrum. Usually, simple boundaries have been assumed such as semi-infinite media or cylinders [10–12], while spherical geometry is of particular interest for electron energy loss in nanoparticles [9,13]. In this study, all effects due to surface excitations and transition radiation [14–16] are neglected assuming an infinite medium.

Starting from the covariant four-potential [17,18] in Fourier space a dispersive, nonlocal wave equation is obtained in

Sec. II by the replacement $c \rightarrow c_n = c/n$, where c is the vacuum velocity of light and the complex index of refraction is defined as $n^2 = \epsilon\mu$, where ϵ is the effective permittivity and μ is the permeability. Since energy losses are small, v_s can be assumed constant and advantage can be made of a frame of reference where the source distribution is at rest. The static potentials, given in Sec. III, differ from the classical approximation by a dispersive Lorentz factor γ_n . The energy loss of a point charge is obtained in Sec. IV and the angle-resolved spectrum of a Drude conductor is discussed in Sec. V. It is shown that Ohmic losses at low energies are enhanced by frequency-dependent length contraction.

II. MAXWELL EQUATIONS

The electric field and the magnetic induction

$$\mathbf{E} = -\nabla\phi - \partial\mathbf{A}/\partial ct, \quad \mathbf{B} = \nabla \times \mathbf{A} \quad (3)$$

are defined in terms of the potentials (ϕ, \mathbf{A}) that form a four-vector [17,18]. The total four-current $(c\rho, \mathbf{j})$ acting as a source term in the Maxwell equations

$$\nabla \cdot \mathbf{E} = 4\pi\rho, \quad c\nabla \times \mathbf{B} = \partial\mathbf{E}/\partial t + 4\pi\mathbf{j} \quad (4)$$

includes the external source $(c\rho_s, \mathbf{j}_s)$ as well as the induced four-current $(c\rho_p, \mathbf{j}_p + \mathbf{j}_m)$ representing the effects of polarization and magnetization. In the Minkowski formulation,

$$\nabla \cdot \mathbf{D} = 4\pi\rho_s, \quad c\nabla \times \mathbf{H} = \partial\mathbf{D}/\partial t + 4\pi\mathbf{j}_s, \quad (5)$$

the inductions are related to the fields by Fourier transformed and dispersive [19] constitutive relations

$$\mathbf{D} = \epsilon\mathbf{E}, \quad \mathbf{B} = \mu\mathbf{H}, \quad (6)$$

allowing the four-current to be written as

$$(c\rho, \mathbf{j}) = (c\rho_s/\epsilon, \mu\mathbf{j}_s + \sigma\mathbf{E}). \quad (7)$$

The total conductivity $\sigma = -i\omega(\epsilon\mu - 1)/4\pi$ is the sum of a term $\sigma_p = -i\omega\chi_e$, due to polarization, and a magnetic contribution $\sigma_m = -i\omega\epsilon\mu\chi_m$ producing the current

$$\mathbf{j}_m = (\mu - 1)\mathbf{j}_s + \sigma_m\mathbf{E}, \quad (8)$$

*Electronic address: jmh@aue.auc.dk

where $\chi_e = (\epsilon - 1)/4\pi$ and $\chi_m = (1 - 1/\mu)/4\pi$ are the electric and magnetic susceptibility, respectively.

The Fourier transform of Eq. (4) can be written as

$$(k^2 - \omega^2/c^2)(\phi, \mathbf{A}) = 4\pi(\rho, \mathbf{j}/c) + (\omega/c, \mathbf{k})(\mathbf{k} \cdot \mathbf{A} - \omega\phi/c), \quad (9)$$

where $(\omega/c, \mathbf{k})$ is the four-wave vector and the scalar four-product $(\omega/c, \mathbf{k}) \cdot (\phi, \mathbf{A})$ appearing in the last term is arbitrary according to the gauge transformation

$$(\phi, \mathbf{A}) \rightarrow (\phi, \mathbf{A}) + i(\omega/c, \mathbf{k})\Phi, \quad (10)$$

where Φ is an arbitrary function. When the four-current (7) is inserted in Eq. (9), it can be seen that this term vanishes in the Lorentz gauge,

$$(\omega/c_n, \mathbf{k}) \cdot (\phi, \mathbf{A}/n) = 0, \quad (11)$$

where $c_n = c/n$ is the phase velocity in the medium and the vector potential is modified according to the fact that ϕ and \mathbf{A} have the same dimension in Gaussian units. The Fourier-transformed potentials are therefore given by the nonlocal wave equation

$$(k^2 - \omega^2/c_n^2)(\phi, \mathbf{A}/n) = 4\pi(\rho_s, \mathbf{j}_s/c_n)/\epsilon, \quad (12)$$

where the factor $1/\epsilon$ accounts for polarization. The modified dispersion relation $\omega = c_n k$ imply that wave vectors are scaled by the complex number n while the frequency is unchanged compared to a plane wave propagating in vacuum.

III. SOURCE REST FRAME

The source, composed of a single charge or a beam [20] of electrons, is assumed at rest in a frame of reference moving at constant velocity v_s relative to the laboratory z axis. In the rest frame, denoted by primes, four-vectors are given by the Lorentz transformation [17]

$$\phi' = \gamma(\phi - \beta A_z), \quad \mathbf{A}'_{\perp} = \mathbf{A}_{\perp}, \quad A'_z = \gamma(A_z - \beta\phi), \quad (13)$$

where the subscript \perp denotes radial components. Since, $\omega' = 0$, the Doppler relation

$$\omega = v_s k_z, \quad (14)$$

corresponding to the Galilean variable $\tilde{z} = z - v_s t$ follows from the Lorentz transformation of frequency while length contraction can be written as $\tilde{z} = z'/\gamma$, or $k_z = \gamma k'_z$. Since the source current is axial $j_s = \rho_s v_s$, the vector potential can be written as $\mathbf{A} = \epsilon\mu\beta\phi$, where the electric potential

$$\phi = 4\pi\rho/(k_{\perp}^2 + k_z^2/\gamma_n^2) \quad (15)$$

is determined by an anisotropic Poisson equation and the dispersive Lorentz factor γ_n is obtained by substituting $\beta_n = n\beta$ in the vacuum expression (1). Compared to the elec-

trostatic approximation $\gamma_n = 1$, the axial length scales are Lorentz contracted by the factor γ_n and propagating waves are possible, if

$$k_{\perp}^2 + k_z^2/\gamma_n^2 = 0. \quad (16)$$

To obtain the potentials in the source rest frame, one observes that Eq. (9) is covariant. Using the Lorentz transformation the Poisson equation

$$k'^2(\phi', \mathbf{A}'_T) = 4\pi(\rho', \mathbf{j}'_m/c) \quad (17)$$

is obtained, where $\mathbf{j}'_p = \mathbf{j}'_s = 0$, and the steady magnetization current \mathbf{j}'_m is responsible for a transverse vector potential $\mathbf{A}'_T = \mathbf{A} - \mathbf{A}_L$, while the longitudinal part $\mathbf{A}_L = \mathbf{k}(\mathbf{k} \cdot \mathbf{A})/k^2$ is arbitrary as can be seen from the gauge transformation (10). The constitutive relations, defined in the medium rest frame, are not covariant, however, and the inverse Lorentz transformation must be used to transform Eq. (7) to the primed system. The Poisson equation (17) becomes anisotropic [22] and the potentials are not simplified by working in the source rest frame. Similar considerations apply to the electromagnetic fields. The electric field $\mathbf{E} = -i(\mathbf{k}_{\perp} + \mathbf{k}_z/\gamma_n^2)\phi$ and the azimuthal magnetic induction $\mathbf{B} = \epsilon\mu\beta \times \mathbf{E}$ transform as

$$\mathbf{E}'_{\perp} = \gamma(\mathbf{E}_{\perp} + \beta \times \mathbf{B}_{\perp}), \quad E'_z = E_z, \quad (18)$$

$$\mathbf{B}'_{\perp} = \gamma(\mathbf{B}_{\perp} - \beta \times \mathbf{E}_{\perp}), \quad B'_z = B_z, \quad (19)$$

with similar relations for \mathbf{D} and \mathbf{H} . Applying the inverse Lorentz transformation, the Minkowski relations [17] follow from Eq. (6), where the radial components can be written as

$$\mathbf{D}'_{\perp}/\gamma_n^2 = \epsilon\mathbf{E}'_{\perp}/\gamma^2 - (\epsilon\mu - 1)\beta \times \mathbf{H}'_{\perp}, \quad (20)$$

$$\mathbf{B}'_{\perp}/\gamma_n^2 = \mu\mathbf{H}'_{\perp}/\gamma^2 + (\epsilon\mu - 1)\beta \times \mathbf{E}'_{\perp}, \quad (21)$$

while $D'_z = \epsilon E'_z$ and $B'_z = \mu H'_z$. Since the medium is moving at velocity $-v_s$, the constitutive relations become bianisotropic [23]. From Ampere's law, $\mathbf{k}' \times \mathbf{H}' = \mathbf{0}$, the magnetic field can be written as the gradient of a scalar function and the relation [24],

$$(\mathbf{k}'_{\perp} + \gamma^2 \mathbf{k}'_z/\gamma_n^2) \cdot \mathbf{H}' = \mathbf{0}, \quad (22)$$

imply $\mathbf{H}' = \mathbf{0}$. While the magnetic field vanishes in the source rest frame, the electric displacement $\mathbf{D}' = \epsilon(\gamma_n^2 \mathbf{E}'_{\perp}/\gamma^2, E'_z)$ gives rise to both a longitudinal electric field and an azimuthal magnetic induction.

IV. ENERGY LOSS

The source-charge distribution is assumed sharply focused along the trajectory

$$\rho_s = Q\rho_{sz}(\tilde{z})\delta(r_{\perp})/2\pi r_{\perp}, \quad (23)$$

where the axial profile ρ_{sz} reduces to a δ function for a point source resulting in the Fourier component, $\rho_s = Q/(2\pi)^3$. The work done against the induced fields can be obtained in either of the frames considered in Sec. III. The static force

density is $\rho'_s \mathbf{E}'(\mathbf{r}')$, where $\mathbf{E}'_{\perp} = \gamma \mathbf{E}_{\perp} / \gamma_n^2$. Inserting Fourier components the integral over the charge distribution can be written as

$$\mathbf{F} = (2\pi)^3 \int -i\mathbf{k} \frac{4\pi |\rho_s|^2 / \epsilon}{\gamma_n^2 k_{\perp}^2 + k_z^2} d\mathbf{k}, \quad (24)$$

using $\rho_s(-k_z) = \rho_s^*(k_z)$. The axial component is the energy loss per unit path length or stopping power. In cylinder coordinates

$$-F_z = \int_0^{\infty} P(k_{\perp}, k_z) k_{\perp} k_z dk_{\perp} dk_z, \quad (25)$$

where a relativistic-loss probability [2] has been defined as

$$P = (2/\pi) Q^2 \text{Im} \left[\frac{-1/\epsilon}{\gamma_n^2 k_{\perp}^2 + k_z^2} \right], \quad (26)$$

using $\epsilon(-k_z) = \epsilon^*(k_z)$ with similar relations for μ and γ_n . The classical probability

$$P_0 = (2/\pi) Q^2 \text{Im} \{-1/\epsilon\} / k^2 \quad (27)$$

is obtained in the limit of small source velocity, $\beta^2 \ll 1$, corresponding to $\gamma_n = 1$. Relativistic corrections caused by a Lorentz factor γ_n different from unity affect the loss probability in proportion to the radial wave vector that in turn is proportional to the deflection angle given by Eq. (2). Detailed information can therefore be obtained from the angle-resolved energy-loss spectrum recorded as a function of k_{\perp} . Electrons passing through the sample with no deflection, $k_{\perp} = 0$, produces a purely classical spectrum and the zero-loss peak, $k_z \rightarrow 0$, diverges as will be discussed in Sec. V B.

The loss function $\text{Im}\{-1/\epsilon\}$ is a positive quantity implying that the imaginary part of the permittivity must be positive while the real part is constrained by the Kramers-Kronig relations [5,6]. In the static limit $\omega \rightarrow 0$ the loss function has to vanish. In a conductor, the real part of the conductivity σ_p approaches a finite value and ϵ_i therefore diverges while ϵ_r vanishes in a dielectric insulator. At high frequencies, the material response approaches that of vacuum, $\epsilon \rightarrow 1$ and $\gamma_n \rightarrow \gamma$.

Assuming a plane wave propagating along the z axis with real k_z and radial wave vector $k_{\perp} = ik_z / \gamma_n$, the constraint $\text{Re}\{1/\gamma_n\} > 0$ must be imposed if Coulomb-like (elliptic) modes are to be radially evanescent, while $\text{Im}\{1/\gamma_n\} < 0$ is required for Cherenkov (hyperbolic) modes to radiate away from the source trajectory [14]. The Lorentz factor γ_n is thus constrained to the first quadrant.

In a transparent medium the refractive index is nearly real. Energy loss due to Cherenkov radiation [25–27] is possible if n is sufficiently large so that γ_n becomes imaginary. The loss probability (26) then has a maximum on the cone, $|\gamma_n| k_{\perp} = k_z$, where the direction of the wave vector is given by $\text{Re}\{\beta_n\} \cos \theta \sim 1$. In general, the diagonal $\text{Re}\{\beta_n^2\} = 1$ in the complex γ_n plane marks the border for Cherenkov losses.

The total charge density induced by a point charge is given as

$$\rho = \frac{Q}{(2\pi)^2} \text{Re} \int \frac{1}{\epsilon} J_0(r_{\perp} k_{\perp}) e^{ik_z \tilde{z}} k_{\perp} dk_{\perp} dk_z, \quad (28)$$

where J_0 is the zero-order Bessel function of the first kind [21]. If the refractive index depends only on frequency, the corresponding potential can be written as

$$\phi = (Q/\pi) \text{Re} \int \frac{1}{\epsilon(k_z)} K_0(r_{\perp} k_z / \gamma_n) e^{ik_z \tilde{z}} dk_z, \quad (29)$$

where K_0 is the zero-order modified Bessel function of the second kind [21,28]. The potential is an asymmetric function of \tilde{z} in order for energy loss to take place and relativistic corrections to the energy spectrum are ultimately related to the shape of Eq. (29) determined by the Lorentz factor γ_n .

V. DRUDE CONDUCTOR

A number of simple metals can be described by the Drude permittivity [29]

$$\epsilon(\omega) = 1 - \omega_p^2 / (\omega^2 + i\nu\omega), \quad (30)$$

where the plasma frequency is given as

$$\omega_p^2 = 4\pi n_0 e^2 / m \quad (31)$$

and n_0 is the density of conduction electrons with effective mass m . Magnetic effects are neglected ($\mu = 1$) and the conductivity is given as

$$4\pi\sigma_p = \omega_p^2 / (\nu - i\omega), \quad (32)$$

where the damping rate ν is assumed small compared to the plasma frequency. The Fermi velocity of electrons is of the order of the Bohr velocity $v_B = e^2 / \hbar$, where $v_B / c \sim 1/137$ and the response of the medium can therefore be treated classically.

The damped plasma resonance gives rise to a peak in the loss function $\text{Im}\{-1/\epsilon\}$ slightly below the plasma frequency and since $\epsilon(\omega_p) \sim i\nu/\omega_p$, to first order, the peak is proportional to ω_p / ν . At low frequencies $\omega^2 \ll \nu^2$, the imaginary part of the permittivity $\epsilon \sim \omega_p^2 (-1 + i\nu/\omega) / \nu^2$ becomes large and the response is dominated by Ohmic dissipation. The loss function decreases linearly with frequency, $\text{Im}\{-1/\epsilon\} \sim \nu\omega / \omega_p^2$, at a rate proportional to the static resistivity.

A. Induced charge

Although the permittivity (30) depends only on frequency spatial dispersion is implied because of the Doppler relation (14). A polarization wake [27,30,31], static in the source rest frame, is formed behind the source. The induced charge is confined to the negative \tilde{z} axis as follows from Eq. (28) using the integral $\int_0^q k J_0(k) dk = q J_1(q)$ and the limit $q J_1(qr) \rightarrow \delta(r)$ for $q \rightarrow \infty$ [28] corresponding to a vanishing microscopic cutoff. The detailed charge profile is determined

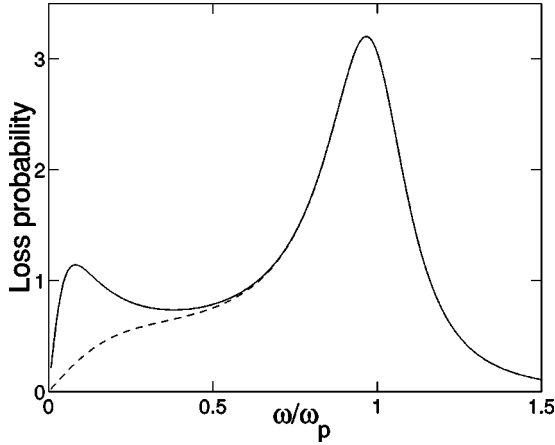


FIG. 1. Angle-resolved energy-loss spectrum of a Drude conductor as a function of reduced frequency at the fixed radial momentum transfer, $k_{\perp}/k_p=0.3$, and damping rate, $\nu/\omega_p=0.3$. The relativistic spectrum at $\beta=0.5$ (solid line) is compared to the classical approximation (dashed line).

by the zeros of ϵ which are in the lower frequency half plane at $\omega = -i\nu/2 \pm \omega_{\nu}$, where $\omega_{\nu}^2 = \omega_p^2 - \nu^2/4$. The integral over axial wave vectors gives the profile

$$\rho_z(\vec{z}) = (\omega_p^2/v_s\omega_{\nu})\exp(\vec{z}/\lambda_{\nu})\sin(2\pi\vec{z}/\lambda), \quad (33)$$

where $\lambda = 2\pi v_s/\omega_{\nu}$ is the wavelength of oscillations in the medium rest frame while $\lambda_{\nu} = 2v_s/\nu$ is the damping length. At small damping rate $\nu^2 \ll \omega_p^2$, the axial wavelength is $\lambda \sim \lambda_p = 2\pi/k_p$, where $k_p = \omega_p/v_s$.

B. Energy-loss spectrum

The relativistic-loss probability (26) is compared to the classical approximation (27) in Fig. 1. The energy-loss spectrum in units of $1/k_p^2$ is shown as a function of reduced frequency, $\omega/\omega_p = k_z/k_p$, at a fixed angle of deflection given by the reduced wave vector $k_{\perp}/k_p = 0.3$.

Near resonance the classical loss probability behaves in a way similar to the loss function, since the denominator k^2 is approximately constant. This regime is also electrostatic in nature since the Lorentz factor given as $\gamma_n^2 \sim 1 + \epsilon(\omega_p)\beta^2$ is close to unity while the refractive index $n \sim \sqrt{\nu/\omega_p}e^{i\pi/4}$ has modulus less than 1. The (real) phase velocity is larger than c and relativistic corrections to the energy-loss spectrum are therefore small.

As the frequency is lowered larger axial length scales are probed [32–34]. At the Drude damping rate $\omega \sim \nu$ corresponding to axial distances on the order of the damping length, the real part of ϵ is large and negative while the imaginary part is large and positive. The Lorentz factor is proportional to ν/ω_p and the $\gamma_n^2 k_{\perp}^2$ term in the denominator of Eq. (26) leads to an increase of the relativistic energy loss over its classical counterpart as shown in Fig. 1.

Electrons that experience no deflection, $k_{\perp} = 0$, will produce a zero-loss peak [32–34] that diverges proportional to ν/ω due to the long-range nature of the Coulomb potential as can be seen from either of the expressions (26) and (27). At

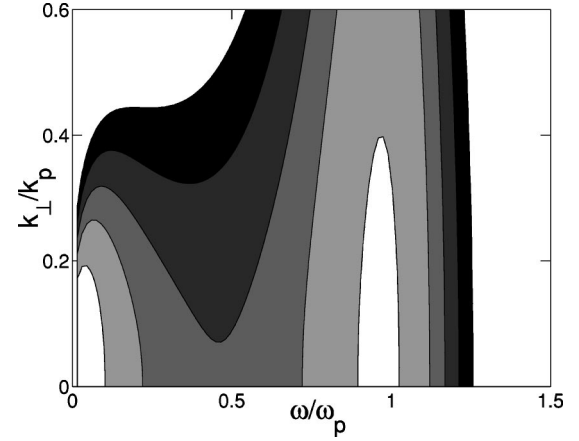


FIG. 2. Contour plot of loss probability (26) as a function of reduced frequency and reduced wave vector k_{\perp}/k_p proportional to the angle of deflection. The parameters are $\nu/\omega_p=0.3$ and $\beta=0.5$.

finite scattering angles, $k_{\perp} > 0$, the linear decrease of the loss function eventually takes over at low frequencies. Given a Lorentz factor that behaves as $\gamma_n \sim \sqrt{i\nu\omega/\beta\omega_p}$, the spectrum decreases as

$$P \sim (\omega/\nu)(\beta k_p/k_{\perp})^4 \quad (34)$$

in the limit $\omega \rightarrow 0$. Compared to the classical expression $P_0 \sim (\nu\omega/\omega_p^2)(k_p/k_{\perp})^2$, the slope of the relativistic curve is larger by the ratio

$$P/P_0 = (\omega_p/\nu)^2 \beta^4 (k_p/k_{\perp})^2, \quad (35)$$

as indicated in Fig. 1. While the classical loss vanishes proportional to the resistivity the relativistic expression (34) shows that the low-energy spectrum decreases proportional to the conductivity. Relativistic corrections, caused by the vector potential, are thus a direct consequence of the current induced at low frequencies.

If the angle of deflection is sufficiently small, the classical probability (27) has a local maximum well below the Drude damping rate at the frequency $\omega \sim \nu k_{\perp}$ corresponding to axial length scales much larger than the damping length. While this condition is not fulfilled in Fig. 1, an additional peak is nevertheless present in the relativistic spectrum due the presence of the factor γ_n in the denominator of the loss probability (26). As shown in Fig. 2 such a peak occurs at low frequencies provided the radial wave vector is smaller than $k_{\perp} \sim 0.45k_p$.

Since plasma frequencies are typically in the ultraviolet, $\hbar\omega_p \sim 15$ eV, the characteristic length λ_p is about 400 Å for 100-keV electrons corresponding to $k_p \sim 0.015$ Å⁻¹. The damping length may be an order of magnitude larger. Present electron-energy-loss spectroscopy instruments have an energy resolution around 0.1 eV while the wave-vector resolution is of the order of 0.05 Å⁻¹. The angular resolution required to discriminate the low-frequency structure apparent in Fig. 2 may therefore be beyond present capabilities.

VI. CONCLUSION

The energy loss of a pointlike charge distribution moving with constant velocity in a dispersive medium has been obtained using macroscopic electrodynamics. The Fourier-transformed potentials are obtained by substituting the characteristic phase velocity $c_n = c/n$ in the corresponding vacuum expressions with sources ρ_s/ϵ and \mathbf{j}_s/ϵ modified to account for polarization. In the source rest frame the fields are static but the constitutive relations are more complicated (bianisotropic) compared to the medium rest frame. In either case, the potentials can be obtained from a nonlocal and anisotropic Poisson equation where the degree of anisotropy is given by the dispersive Lorentz factor γ_n .

As an example, the energy-loss probability of a simple Drude metal has been calculated as a function of radial momentum transfer. Although the single-pole permittivity (30) includes only temporal dispersion the angle-resolved spectrum does show relativistic corrections. While energy loss near the plasma resonance is essentially a classical process since the phase velocity is large and the Lorentz factor is close to unity, retardation effects are observed at lower energies where the phase velocity in the medium becomes small compared to c . The small value of the Lorentz factor γ_n

effectively increases the radial length scale over which the medium is excited thereby enhancing the relativistic spectrum over its classical counterpart. The linear variation observed at energies well below $\hbar\nu$ due to Ohmic dissipation becomes more steep and a possible second maximum occurring for small scattering angles becomes more pronounced when relativistic effects are taken into account.

While the resolution needed to observe the macroscopic behavior described above cannot be obtained in a TEM experiment using a thin metal film, the composite metallic structures recently fabricated [35] may provide a possible alternative. On a macroscopic length scale the effective dielectric function is of the form (30) with plasma frequency in the microwave region [36,37], and since the structure can be made of thin wires in vacuum small momentum excitations may be probed using ballistic electrons. A further interesting aspect is that metallic structures of this type can be designed with exotic magnetic properties [38].

ACKNOWLEDGMENTS

Discussions with J.H. Pedersen and P. Naamansen are gratefully acknowledged.

-
- [1] P.M. Echenique, F. Flores, and R.H. Ritchie, in *Dynamic Screening of Ions in Condensed Matter*, edited by H. Ehrenreich and D. Turnbull, Solid State Physics Vol. 43 (Academic, New York, 1990).
- [2] E. Fermi, Phys. Rev. **57**, 485 (1940); R.H. Ritchie, *ibid.* **106**, 874 (1957); J. Neufeld and R.H. Ritchie, *ibid.* **98**, 1632 (1955); **99**, 1125 (1955).
- [3] H. Raether, *Excitation of Plasmons and Interband Transitions by Electrons*, Springer Tracts in Modern Physics Vol. 88 (Springer, Berlin, 1980).
- [4] R.F. Egerton, *Electron Energy-Loss Spectroscopy in the Electron Microscope*, 2nd ed. (Plenum, New York, 1996).
- [5] J.D. Jackson, *Classical Electrodynamics*, 2nd ed. (Wiley, New York, 1975).
- [6] L.D. Landau and E. M. Lifshitz, *Electrodynamics of Continuous Media* (Pergamon Press, Oxford, 1975).
- [7] E. Kröger, Z. Phys. **216**, 115 (1968); **235**, 403 (1970); F. Forstmann, *ibid.* **217**, 416 (1968); C. von Festenberg, *ibid.* **227**, 453 (1969).
- [8] R. Garcia-Molina, A. Gras-Marti, A. Howie, and R.H. Ritchie, J. Phys. C **18**, 5335 (1985); P. Moreau, N. Brun, C.A. Walsh, C. Colliex, and A. Howie, Phys. Rev. B **56**, 6774 (1997).
- [9] F.J. García de Abajo and A. Howie, Phys. Rev. Lett. **80**, 5180 (1998); F.J. García de Abajo, Phys. Rev. B **59**, 3095 (1999).
- [10] J.B. Pendry and L. Martin-Moreno, Phys. Rev. B **50**, 5062 (1994).
- [11] P.M. Echenique, J. Bausells, and A. Rivacoba, Phys. Rev. B **35**, 1521 (1987); A. Rivacoba, N. Zabala, and P.M. Echenique, Phys. Rev. Lett. **69**, 3362 (1992).
- [12] D. De Zutter and D. De Vleeschauwer, J. Appl. Phys. **59**, 4146 (1986); N. Zabala, A. Rivacoba, and P.M. Echenique, Surf. Sci. **209**, 465 (1989); C.A. Walsh, Philos. Mag. B **63**, 1063 (1991).
- [13] H. Cohen, T. Maniv, R. Tenne, Y.R. Hacoheh, O. Stephan, and C. Colliex, Phys. Rev. Lett. **80**, 782 (1998); **83**, 659 (1999); P.M. Echenique, A. Howie, and R.H. Ritchie, *ibid.* **83**, 658 (1999).
- [14] V.L. Ginzburg, *Applications of Electrodynamics in Theoretical Physics and Astrophysics* (Gordon and Breach, New York, 1989).
- [15] N. Yamamoto, H. Sugiyama, and A. Toda, Proc. R. Soc. London, Ser. A **452**, 2279 (1996); N. Yamamoto, A. Toda, and K. Araya, J. Electron Microsc. **45**, 64 (1996); N. Yamamoto and A. Toda, Scanning Microsc. **9**, 669 (1995).
- [16] L.L. DeRaad, Wu-yang Tsai, and T. Erber, Phys. Rev. D **18**, 2152 (1978); Wu-yang Tsai, J. Nearing, and L.L. DeRaad, *ibid.* **21**, 3428 (1980).
- [17] Wolfgang Pauli, *Theory of Relativity* (Dover, New York, 1981).
- [18] J. Cohn, Ann. Phys. (N.Y.) **114**, 467 (1978); F. Hartemann and Z. Toffano, Phys. Rev. A **41**, 5066 (1990).
- [19] G.S. Agarwal, D.N. Pattanayak, and E. Wolf, Phys. Rev. B **10**, 1447 (1974); B.J. Hoenders and D.N. Pattanayak, Phys. Rev. D **13**, 282 (1976); D. L Johnson and P.R. Rimbey, Phys. Rev. B **14**, 2398 (1976).
- [20] D.W. Rule and M.H. Cha, Phys. Rev. A **24**, 55 (1981).
- [21] G.N. Watson, *A Treatise on the Theory of Bessel Functions*, 2nd ed. (Cambridge University Press, New York, 1995).
- [22] G.P. Sastry, Am. J. Phys. **44**, 707 (1976); **46**, 554 (1978); G.P. Sastry and D. Chowdhury, Proc. R. Soc. London, Ser. A **374**, 531 (1981).
- [23] J.A. Kong, *Theory of Electromagnetic Waves* (Wiley, New York, 1975).
- [24] J. Van Bladel, *Relativity and Engineering* (Springer, New York, 1984).
- [25] F.R. Buskirk and J.R. Neighbours, Phys. Rev. A **28**, 1531

- (1983); **31**, 3750 (1985); **34**, 3470 (1986).
- [26] G.S. Smith, Am. J. Phys. **61**, 147 (1993); T.W. Hertel and G.S. Smith, IEEE Trans. Antennas Propag. **40**, 165 (2000).
- [27] G.N. Afanasiev and V.G. Kartavenko, J. Phys. D **31**, 2760 (1998); G.N. Afanasiev, V.G. Kartavenko, and E.N. Magar, Physica B **269**, 95 (1999); V.G. Kartavenko, G.N. Afanasiev, and W. Greiner, *ibid.* **271**, 192 (1999).
- [28] I.S. Gradshteyn and I.M. Ryzik, *Tables of Integrals, Series and Products* (Academic Press, New York, 1965).
- [29] N.W. Ashcroft and N.D. Mermin, *Solid State Physics* (Holt-Saunders, New York, 1976).
- [30] V.N. Neelavathi, R.H. Ritchie, and W. Brandt, Phys. Rev. Lett. **33**, 302 (1974); R.H. Ritchie, W. Brandt, and P.M. Echenique, Phys. Rev. B **14**, 4808 (1976); P.M. Echenique, R.H. Ritchie, and W. Brandt, *ibid.* **20**, 2567 (1979); A. Mazarro, P.M. Echenique, and R.H. Ritchie, *ibid.* **27**, 4117 (1983).
- [31] Z. Vager and D.S. Gemmell, Phys. Rev. Lett. **37**, 1352 (1976); S.K. Mtingwa, Phys. Rev. A **37**, 1668 (1988).
- [32] G.P. Sastry and B.K. Parida, Phys. Rev. D **18**, 3025 (1978).
- [33] L. Schächter, Phys. Rev. E **53**, 6427 (1996); L. Schächter and D. Schieber, Nucl. Instrum. Methods Phys. Res. A **388**, 8 (1997); D. Schieber and L. Schächter, Phys. Rev. E **57**, 6008 (1998).
- [34] G.F. Bertsch, H. Esbensen, and B.W. Reed, Phys. Rev. B **58**, 14 031 (1998).
- [35] J.B. Pendry, A.J. Holden, D.J. Robbins, and W.J. Stewart, J. Phys.: Condens. Matter **10**, 4785 (1998).
- [36] J.B. Pendry, A.J. Holden, W.J. Stewart, and I. Youngs, Phys. Rev. Lett. **76**, 4773 (1996); **78**, 4136 (1997); S.A. Mikhailov, *ibid.* **78**, 4135 (1997).
- [37] R.M. Walser, A.P. Valanju, and P.M. Valanju, Phys. Rev. Lett. **87**, 119701 (2001).
- [38] J.B. Pendry, Phys. World **13**(6), 27 (2000); A.K. Sarychev, R.C. McPhedran, and V.M. Shalaev, Phys. Rev. B **62**, 8531 (2000); R.A. Shelby, D.R. Smith, and S. Schultz, Science **292**, 77 (2001).